

DISCRETE CONSTANT MEAN CURVATURE SURFACES AND THEIR INDEX

KONRAD POLTHIER AND WAYNE ROSSMAN

ABSTRACT. We define triangulated piecewise linear constant mean curvature surfaces using a variational characterization. These surfaces are critical for area amongst continuous piecewise linear variations which preserve the boundary conditions, the simplicial structures, and (in the nonminimal case) the volume to one side of the surfaces. We then find explicit formulas for complete examples, such as discrete minimal catenoids and helicoids.

We use these discrete surfaces to study the index of unstable minimal surfaces, by numerically evaluating the spectra of their Jacobi operators. Our numerical estimates confirm known results on the index of some smooth minimal surfaces, and provide additional information regarding their area-reducing variations. The approach here deviates from other numerical investigations in that we add geometric interpretation to the discrete surfaces.

1. INTRODUCTION

Smooth submanifolds, and surfaces in particular, with constant mean curvature (CMC) have a long history of study, and modern work in this field relies heavily on geometric and analytic machinery which has evolved over hundreds of years. However, nonsmooth surfaces are also natural mathematical objects, even though there is less machinery available for studying them. (Consider M. Gromov's approach of doing geometry using only a set with a measure and a measurable distance function [9].)

Here we consider piecewise linear triangulated surfaces (we call them "discrete surfaces"), which have been brought more to the forefront of geometrical research by computer graphics. We define CMC for discrete surfaces in \mathbb{R}^3 so that they are critical for volume-preserving variations, just as smooth CMC surfaces are. Discrete CMC surfaces have both interesting differences from and similarities with smooth ones. For example, they are different in that smooth minimal graphs in \mathbb{R}^3 over a bounded domain are stable, whereas discrete minimal graphs can be highly unstable. We will explore properties like this in section 2.

In section 3 we will see some ways in which these two types of surfaces are similar. We will see that: a discrete catenoid has an explicit description in terms of the hyperbolic cosine function, just as the smooth catenoid has; and a discrete helicoid can be described with the hyperbolic sine function, just as a conformally parametrized smooth helicoid is; and there are discrete Delaunay surfaces which have translational periodicities, just as smooth Delaunay surfaces have.

Pinkall and Polthier [17] used Dirichlet energy and a numerical minimization procedure to find discrete minimal surfaces. In this work, we rather have the goal to describe discrete minimal surfaces as explicitly as possible, and thus we are limited to the more fundamental examples, for example the discrete minimal catenoid and

helicoid. We note that these explicit descriptions will be useful test candidates when implementing a procedure that we describe in the next paragraphs.

Discrete surfaces have finite dimensional spaces of admissible variations, therefore the study of linear differential operators on the variation spaces reduces to the linear algebra of matrices. This advantage over smooth surfaces with their infinite dimensional variation spaces makes linear operators easier to handle in the discrete case.

This suggests that a useful procedure for studying the spectra of the linear Jacobi operator in the second variation formula of smooth CMC surfaces is to consider the corresponding spectra of discrete CMC approximating surfaces. Although similar to the finite element method in numerical analysis, here the finite element approximations will have geometric and variational meaning in their own right.

As an example, consider how one finds the index (the number of negative points in the spectrum) of a smooth minimal surface. The standard approach is to replace the metric of the surface with the metric obtained by pulling back the spherical metric via the Gauss map. This approach can yield the index: for example, the indexes of a complete catenoid and a complete Enneper surface are 1 ([7]), the index of a complete Jorge-Meeks n -noid is $2n - 3$ ([12], [11]) and the index of a complete genus k Costa-Hoffman-Meeks surface is $2k + 3$ for every $k \leq 37$ ([14], [13]). However, this approach does not yield the eigenvalues and eigenfunctions on compact portions of the original minimal surfaces, as the metric has been changed. It would be interesting to know the eigenfunctions associated to negative eigenvalues, since these represent the directions of variations that reduce area. The above procedure of approximating by discrete surfaces can provide this information.

In sections 5 and 6 we establish some tools for studying the spectrum of discrete CMC surfaces. Then we test the above procedure on two standard cases – a (minimal) rectangle, and a portion of a smooth minimal catenoid bounded by two circles. In these two cases we know the spectra of the smooth surfaces (section 4), and we know the discrete minimal surfaces as well (section 3), so we can check that the above procedure produces good approximations for the eigenvalues and smooth eigenfunctions (section 7), which indeed must be the case, by the theory of the finite element method [4], [8]. With these successful tests, we go on to consider cases where we do not apriori know what the smooth eigenfunctions should be, such as the Jorge-Meeks 3-noid and the genus 1 Costa surface (section 7).

We note that the above procedure can also be implemented using discrete approximating surfaces which are found only numerically and not explicitly, such as surfaces found by the method in [17]. And in fact, we use the method in [17] to find approximating surfaces for the 3-noid and Enneper surface and Costa surface.

We note also that Ken Brakke's surface evolver software [3] is an efficient tool for numerical index calculations using the same discrete ansatz. Our main emphasis here is to provide explicit formulations for the discrete Jacobi operator and other geometric properties of discrete surfaces.

2. DISCRETE MINIMAL AND CMC SURFACES

We start with a variational characterization of discrete minimal and discrete CMC surfaces. This characterization will allow us to construct explicit examples of *unstable* discrete CMC surfaces. (Note that merely finding minima for area with respect to a volume constraint would not suffice for this, as that would produce only

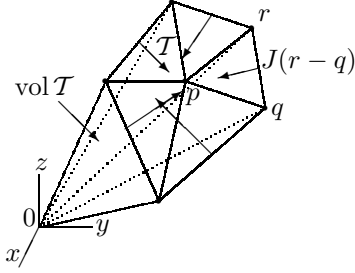


FIGURE 1. The vectors $J(r-q)$ whose sum form the gradient of discrete area, as in Equation (1).

stable examples.) We will later use these discrete CMC surfaces for our numerical spectra computations.

The following definitions for discrete surfaces and their variations work equally well in any ambient space \mathbb{R}^n , but for simplicity we restrict to \mathbb{R}^3 .

Definition 2.1. A discrete surface in \mathbb{R}^3 is a triangular mesh \mathcal{T} which has the topology of an abstract 2-dimensional simplicial surface K combined with a geometric C^0 realization in \mathbb{R}^3 that is piecewise linear on each simplex. The geometric realization $|K|$ is determined by a set of vertices $\mathcal{V} = \{p_1, \dots, p_m\} \subset \mathbb{R}^3$, and \mathcal{T} can be identified with the pair (K, \mathcal{V}) . The simplicial complex K represents the connectivity of the mesh. The 0, 1, and 2 dimensional simplices of K represent the vertices, edges, and triangles of the discrete surface.

Let $T = (p, q, r)$ denote an oriented triangle of \mathcal{T} with vertices $p, q, r \in \mathcal{V}$. Let \overline{pq} denote an edge of T with endpoints $p, q \in \mathcal{V}$.

For $p \in \mathcal{V}$, let $\text{star}(p)$ denote the triangles of \mathcal{T} that contain p as a vertex. For an edge \overline{pq} , let $\text{star}(\overline{pq})$ denote the (at most two) triangles of \mathcal{T} that contain \overline{pq} as an edge.

Definition 2.2. Let $\mathcal{V} = \{p_1, \dots, p_m\}$ be the set of vertices of a discrete surface \mathcal{T} . A variation $\mathcal{T}(t)$ of \mathcal{T} is defined as a C^2 variation of the vertices p_i

$$p_i(t) : [0, \epsilon) \rightarrow \mathbb{R}^3 \text{ so that } p_i(0) = p_i \quad \forall i = 1, \dots, m.$$

The straightness of the edges and the flatness of the triangles are preserved as the vertices move.

In the smooth situation, the variation at interior points is typically restricted to normal variation, since the tangential part of the variation only performs a reparametrization of the surface. However, on discrete surfaces there is an ambiguity in the choice of normal vectors at the vertices, so we allow arbitrary variations. But we will later see (section 7) that our experimental results can accurately estimate normal variations of a smooth surface when the discrete surface is a close approximation to the smooth surface.

In the following we derive the evolution equations for some basic entities under surface variations.

The area of a discrete surface is

$$\text{area}(\mathcal{T}) := \sum_{T \in \mathcal{T}} \text{area } T,$$

where $\text{area } T$ denotes the Euclidean area of the triangle T as a subset of \mathbb{R}^3 .

Let $\mathcal{T}(t)$ be a variation of a discrete surface \mathcal{T} . At each vertex p of \mathcal{T} , the gradient of area is

$$(1) \quad \nabla_p \text{area } \mathcal{T} = \frac{1}{2} \sum_{T=(p,q,r) \in \text{star } p} J(r-q),$$

where J is rotation of angle $\frac{\pi}{2}$ in the plane of each oriented triangle T . The first derivative of the surface area is then given by the chain rule

$$(2) \quad \frac{d}{dt} \text{area } \mathcal{T} = \sum_{p \in \mathcal{V}} \langle p', \nabla_p \text{area } \mathcal{T} \rangle.$$

The volume of an oriented surface \mathcal{T} is the oriented volume enclosed by the cone of the surface over the origin in \mathbb{R}^3

$$\text{vol } \mathcal{T} := \frac{1}{6} \sum_{T=(p,q,r) \in \mathcal{T}} \langle p, q \times r \rangle = \frac{1}{3} \sum_{T=(p,q,r) \in \mathcal{T}} \langle \vec{N}, p \rangle \cdot \text{area } T,$$

where p is any of the three vertices of the triangle T and $\vec{N} = (q-p) \times (r-p) / |(q-p) \times (r-p)|$ is the oriented normal of T . It follows that

$$(3) \quad \nabla_p \text{vol } \mathcal{T} = \sum_{T=(p,q,r) \in \text{star } p} q \times r / 6$$

and

$$(4) \quad \frac{d}{dt} \text{vol } \mathcal{T} = \sum_{p \in \mathcal{V}} \langle p', \nabla_p \text{vol } \mathcal{T} \rangle.$$

Remark 2.1. Note also that $\nabla_p \text{vol } \mathcal{T} = \sum_{T=(p,q,r) \in \text{star } p} (2 \cdot \text{area } T \cdot \vec{N} + p \times (r-q)) / 6$. Furthermore, if p is an interior vertex, then the boundary of $\text{star } p$ is closed and $\sum_{T \in \text{star } p} p \times (r-q) = 0$. Hence the $q \times r$ in Equation (3) can be replaced with $2 \cdot \text{area } T \cdot \vec{N}$ whenever p is an interior vertex.

In the smooth case, a minimal surface is critical with respect to area for any variation that fixes the boundary, and a CMC surface is critical with respect to area for any variation that preserves volume and fixes the boundary. We wish to define discrete CMC surfaces so that they have the same variational properties for the same types of variations. So we will consider variations $\mathcal{T}(t)$ of \mathcal{T} that fix the boundary $\partial \mathcal{T}$ and that additionally preserve volume in the nonminimal case, which we call *permissible variations*. The condition that makes a discrete surface area-critical for any permissible variation is expressed in the following definition.

Definition 2.3. A discrete surface has constant mean curvature (CMC) if there exists a constant H so that $\nabla_p \text{area} = H \nabla_p \text{vol}$ for all interior vertices p . If $H = 0$ then it is minimal.

This definition for discrete minimality has been used in [17]. In contrast, our definition of discrete CMC surfaces differs from [15], where CMC surfaces are characterized algorithmically using discrete minimal surfaces in S^3 and a conjugation transformation. Compare also [2] for a definition via discrete integrable systems which lacks variational properties.

Remark 2.2. *If \mathcal{T} is a discrete minimal surface that contains a simply-connected discrete subsurface \mathcal{T}' that lies in a plane, then it follows easily from Equation (1) that the discrete minimality of \mathcal{T} is independent of the choice of triangulation of the trace of \mathcal{T}' .*

2.0.1. *Notation from the Theory of Finite Elements.* Consider a vector-valued function $v_{p_j} \in \mathbb{R}^3$ defined on the n interior vertices $\mathcal{V}_{int} = \{p_1, \dots, p_n\}$ of \mathcal{T} . (We may extend this function to the boundary vertices of \mathcal{T} as well, by assuming $v_p = \vec{0} \in \mathbb{R}^3$ for each boundary vertex p .) The vectors v_{p_j} are the variation vector field of any boundary-fixing variation of the form

$$(5) \quad p_j(t) = p_j + t \cdot v_{p_j} + \mathcal{O}(t^2),$$

that is, $p_j'(0) = v_{p_j}$. We define the vector $\vec{v} \in \mathbb{R}^{3n}$ by

$$(6) \quad \vec{v}^t = (v_{p_1}^t, \dots, v_{p_n}^t).$$

The variation vector field \vec{v} can be naturally extended to a piece-wise linear continuous \mathbb{R}^3 -valued function v on \mathcal{T} , with v in the following vector space:

Definition 2.4. *Define S_h of the discrete surface \mathcal{T} to be*

$$S_h := \{v : \mathcal{T} \rightarrow \mathbb{R}^3 \mid v \in C^0(\mathcal{T}), v \text{ is linear on each } T \in \mathcal{T} \text{ and } v|_{\partial\mathcal{T}} = 0\}.$$

This space is named S_h , as in the theory of finite elements. Note that any component function of any function $v \in S_h$ has bounded Sobolev H^1 norm.

For each triangle $T = (p, q, r)$ in \mathcal{T} and each $v \in S_h$,

$$(7) \quad v|_T = v_p \psi_p + v_q \psi_q + v_r \psi_r,$$

where $\psi_p : \mathcal{T} \rightarrow \mathbb{R}$ is the *head function* on \mathcal{T} which is 1 at p and is 0 at all other vertices of \mathcal{T} and extends linearly to all of \mathcal{T} in the unique way. The functions ψ_{p_j} form a basis (with scalars in \mathbb{R}^3) for the $3n$ -dimensional space S_h .

2.0.2. *Non-Uniqueness of Discrete Minimal Disks.* Uniqueness of a bounded minimal surface with a given boundary ensures that it is stable. For smooth minimal surfaces, uniqueness can sometimes be decided using the maximum principle of elliptic equations, which ensures that the minimal surface is contained in the convex hull of its boundary, and, if the boundary has a 1-1 projection to a convex planar curve, then it is unique for that boundary and is a minimal graph. The maximum principle also shows that any minimal graph is unique even when the projection of its boundary is not convex. More generally, stability still holds when the surface merely has a Gauss map image contained in a hemisphere, as shown in [1] (although their proof employs tools other than the maximum principle).

However, such statements do not hold for discrete minimal surfaces. Consider the surface shown in the left-hand side of Figure 2, whose height function has a local maximum at an interior vertex. This example does not lie in the convex hull of its boundary and thereby disproves the general existence of a discrete version of the maximum principle. Also, the three surfaces on the right-hand side in Figure 3 are all minimal graphs over an annular domain with the same boundary contours and the same simplicial structure, and yet they are not the same surfaces, hence graphs with given simplicial structure are not unique. And the left-hand surface in Figure 3 is a surface whose Gauss map is contained in a hemisphere but which is unstable (this surface is not a graph) – another example of this property is the first

annular surface in Figure 3, which is also unstable. (We define stability of discrete CMC surfaces in section 5).

The influence of the discretization on nonuniqueness, like as in the annular examples of Figure 3, can also be observed in a more trivial way for a discrete minimal graph over a simply connected convex domain. The two surfaces on the right-hand side of Figure 2 have the same trace, i.e. they are identical as geometric surfaces, but they are different as discrete surfaces. Interior vertices may be freely added and moved inside the middle planar square without affecting minimality (see Remark 2.2).

In contrast to existence of these counterexamples we believe that some properties of smooth minimal surfaces remain true in the discrete setting. We say that a discrete surface is a disk if it is homeomorphic to a simply connected domain.

Conjecture 2.1. *Let $\mathcal{T} \subset \mathbb{R}^3$ be a discrete minimal disk whose boundary projects injectively to a convex planar polygonal curve, then \mathcal{T} is a graph over that plane.*

The authors were able to prove this conjecture with the extra assumption that all the triangles of the surface are acute, using the fact that the maximum principle (a height function cannot attain a strict interior maximum) actually does hold when all triangles are acute.

One can ask if a discrete minimal surface \mathcal{T} with given simplicial structure and boundary is unique if it has a 1-1 perpendicular or central projection to a convex polygonal domain in a plane. The placement of the vertices need not be unique, as we saw in Remark 2.2, however, one can consider if there is uniqueness in the sense that the trace of \mathcal{T} in \mathbb{R}^3 is unique:

Conjecture 2.2. *Let $\Gamma \subset \mathbb{R}^3$ be a polygonal curve that either \mathcal{A} : projects injectively to a convex planar polygonal curve, or \mathcal{B} : has a 1-1 central projection from a point $p \in \mathbb{R}^3$ to a convex planar polygonal curve. Let K be a given abstract simplicial disk, and let $\gamma : \partial K \rightarrow \Gamma$ be a given piecewise linear map. If \mathcal{T} is a discrete minimal surface that is a geometric realization of K so that the map $\partial K \rightarrow \partial \mathcal{T}$ equals γ , then the trace of \mathcal{T} in \mathbb{R}^3 is uniquely determined. Furthermore, \mathcal{T} is a graph in the case \mathcal{A} , and \mathcal{T} is contained in the cone of Γ over p in the case \mathcal{B} .*

We have the following weaker form of Conjecture 2.2, which follows from Corollary 5.1 of section 5 in the case that there is only one interior vertex:

Conjecture 2.3. *If a discrete minimal surface is a graph over a convex polygonal domain, then it is stable.*

3. EXPLICIT DISCRETE SURFACES

Here we describe explicit discrete catenoids and helicoids, which seem to be the first explicitly known nontrivial complete discrete minimal surfaces (with minimality defined variationally).

3.1. Discrete Minimal Catenoids. To derive an explicit formula for embedded complete discrete minimal catenoids, we choose the vertices to lie on congruent planar polygonal meridians, with the meridians placed so that the traces of the surfaces will have dihedral symmetry. We will find that the vertices of a discrete meridian lie equally spaced on a smooth hyperbolic cosine curve. Furthermore, these discrete catenoids will converge uniformly in compact regions to the smooth catenoid as the mesh is made finer.

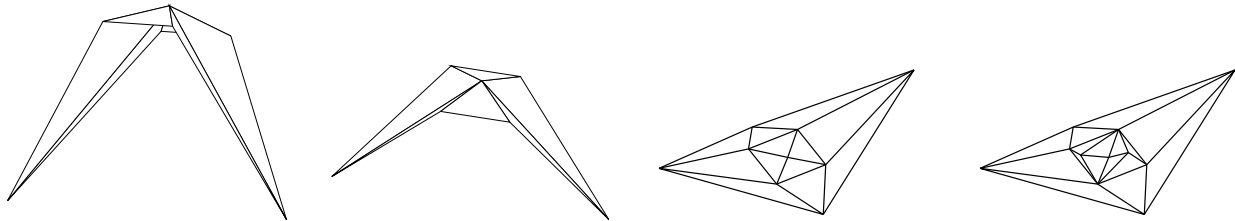


FIGURE 2. Two views on the left-hand side of a discrete minimal surface that defies the maximum principle. The two discrete minimal surfaces on the right-hand side with boundary vertices $(x, 0, z_1)$, $(-x, 0, z_1)$, $(0, y, z_2)$, and $(0, -y, z_2)$ in \mathbb{R}^3 have the same trace in \mathbb{R}^3 but have different simplicial structures. Another surprising feature of these examples is that the innermost triangles form a square, regardless of the values of $x, y, z_1 \neq z_2$.

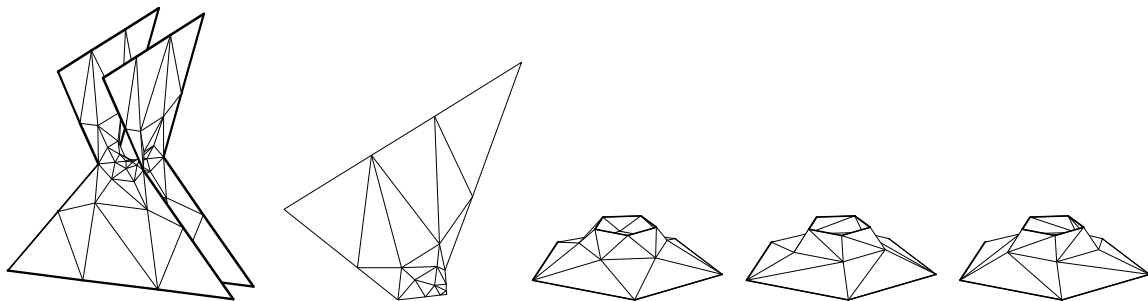


FIGURE 3. Two unstable and two stable discrete minimal surfaces in \mathbb{R}^3 . The first figure on the left is unstable, even though it is locally a graph over a horizontal plane, in the sense that the third coordinate of the normal vector to the surface is never zero. The second figure on the left is one of the four congruent pieces of the first figure. The middle figure (the leftmost annular graph) is unstable, even though it is a graph over an annular polygonal region in a horizontal plane; it has area-reducing variations that can deform to either of the last two stable minimal surfaces on the right, which have the same simplicial structure.

We begin with a lemma that prepares the construction of the vertical meridian of the discrete minimal catenoid, by successively adding one horizontal ring after another starting from an initial ring. Since our construction will lead to pairwise coplanar triangles, the star of each individual vertex can be made to consist of four triangles (see Remark 2.2). We now derive an explicit representation of the position of a vertex surrounded by four such triangles in terms of the other four vertex positions. The center vertex is assumed to be coplanar with each of the two pairs of two opposite vertices, with those two planes becoming the plane of the vertical meridian and the horizontal plane containing a dihedrally symmetric polygonal ring (consisting of edges of the surface). See Figure 4.

Lemma 3.1. *Suppose we have four vertices $p = (d, 0, e)$, $q_1 = (d \cos \theta, -d \sin \theta, e)$, $q_2 = (a, 0, b)$, and $q_3 = (d \cos \theta, d \sin \theta, e)$, for given real numbers a, b, d, e , and angle θ so that $b \neq e$. Then there exists a choice of real numbers x and y and a*

fifth vertex $q_4 = (x, 0, y)$ so that the discrete surface formed by the four triangles (p, q_1, q_2) , (p, q_2, q_3) , (p, q_3, q_4) , and (p, q_4, q_1) is minimal, i.e.

$$\nabla_p \text{area}(\text{star } p) = 0,$$

if and only if

$$2ad > \frac{(e-b)^2}{1 + \cos \theta}.$$

Furthermore, when x and y exist, they are unique and must be of the form

$$\begin{aligned} x &= \frac{2(1 + \cos \theta)d^3 + (a + 2d)(e - b)^2}{2ad(1 + \cos \theta) - (e - b)^2}, \\ y &= 2e - b. \end{aligned}$$

Proof. First we note that the assumption $b \neq e$ is necessary. If $b = e$, then one may choose $y = b$, and then there is a free 1-parameter family of choices of x , leading to a trivial planar surface.

For simplicity we apply a vertical translation and a homothety about the origin of \mathbb{R}^3 to normalize $d = 1$, $e = 0$, and by doing a reflection if necessary, we may assume $b < 0$. Let $c = \cos \theta$ and $s = \sin \theta$.

We derive conditions for the coordinate components of $\nabla_p \text{area}$ to vanish. The second component vanishes by symmetry of star p . Using the definitions

$$c_1 := \frac{(a-1)s^2 - b^2(1-c)}{\sqrt{2b^2(1-c) + (a-1)^2s^2}}, \quad c_2 := \frac{ab+b}{\sqrt{2b^2(1-c) + (a-1)^2s^2}},$$

the first (resp. third) component of $\nabla_p \text{area}$ vanishes if

$$(8) \quad c_1 = \frac{y^2(1-c) - (x-1)s^2}{\sqrt{2y^2(1-c) + (x-1)^2s^2}}, \quad \text{resp.} \quad c_2 = \frac{-(x-1)y - 2y}{\sqrt{2y^2(1-c) + (x-1)^2s^2}}.$$

Dividing one of these equations by the other we obtain

$$(9) \quad x - 1 = \frac{c_2y(1-c) + 2c_1}{c_2s^2 - c_1y}y,$$

so x is determined by y . It now remains to determine if one can find y so that $c_2s^2 - c_1y \neq 0$. If $x - 1$ is chosen as in equation (9), then the first minimality condition of equation (8) holds if and only if the second one holds as well. So we only need to insert this value for $x - 1$ into the first minimality condition and check for solutions y . When $c_1 \neq 0$, we find that the condition becomes

$$1 = \frac{c_2s^2 - c_1y}{|c_2s^2 - c_1y|} \frac{y}{|y|} \frac{-(1-c)y^2 - 2s^2}{\sqrt{2(1-c)c_2^2s^4 + 4c_1^2s^2 + (2(1-c)c_1^2 + s^2(1-c)^2c_2^2)y^2}}.$$

Since $-(1-c)y^2 - 2s^2 < 0$, note that this equation can hold only if $c_2s^2 - c_1y$ and y have opposite signs, so the equation becomes

$$1 = \frac{(1-c)y^2 + 2s^2}{\sqrt{2(1-c)c_2^2s^4 + 4c_1^2s^2 + (2(1-c)c_1^2 + s^2(1-c)^2c_2^2)y^2}},$$

which simplifies to

$$1 = \frac{\sqrt{(1-c)y^2 + 2s^2}}{\sqrt{(1-c)c_2^2s^2 + 2c_1^2}}.$$

This implies y^2 is uniquely determined. Inserting the value

$$y = \pm b,$$

one finds that the above equation holds. When $y = b < 0$, we find that $c_2s^2 - c_1y < 0$, which is impossible. When $y = -b > 0$, we find that $c_2s^2 - c_1y < 0$ if and only if $2a(1+c) > b^2$. And when $y = -b$ and $2a(1+c) > b^2$, we have the minimality condition when

$$x = \frac{2 + 2c + ab^2 + 2b^2}{2a + 2ac - b^2}.$$

Inverting the transformation we did at the beginning of this proof brings us back to the general case where d and e are not necessarily 1 and 0, and the equations for x and y become as stated in the lemma.

When $c_1 = 0$, we have $(a-1)(1+c) = b^2$ and $(x-1)(1+c) = y^2$, so, in particular, we have $a > 1$ and therefore $2a(1+c) > b^2$. The right-hand side of equation (8) implies $y = -b$ and $x = a$. Again, inverting the transformation from the beginning of this proof, we have that x and y must be of the form in the lemma for the case $c_1 = 0$ as well. \square

The next lemma provides a necessary and sufficient condition for when two points lie on a scaled cosh curve, a condition that is identical to that of the previous lemma. That these conditions are the same is crucial to the proof of the upcoming theorem.

Lemma 3.2. *Given two points (a, b) and (d, e) in \mathbb{R}^2 with $b \neq e$, and an angle θ with $|\theta| < \pi$, there exists an r so that these two points lie on some vertical translate of the modified cosh curve*

$$\gamma(t) = \left(r \cosh \left[\frac{t}{e-b} \operatorname{arccosh} \left(1 + \frac{1}{r^2} \frac{(e-b)^2}{1+\cos\theta} \right) \right], t \right), \quad t \in \mathbb{R},$$

if and only if $2ad > \frac{(e-b)^2}{1+\cos\theta}$.

Proof. Define $\hat{\delta} = \frac{e-b}{\sqrt{1+\cos\theta}}$. Without loss of generality, we may assume $0 < a \leq d$ and $e > 0$, and hence $-e \leq b < e$. If the points (a, b) and (d, e) both lie on the curve $\gamma(t)$, then

$$\operatorname{arccosh} \left(1 + \frac{\hat{\delta}^2}{r^2} \right) = \operatorname{arccosh} \left(\frac{d}{r} \right) - \operatorname{sign}(b) \cdot \operatorname{arccosh} \left(\frac{a}{r} \right),$$

where $\operatorname{sign}(b) = 1$ if $b \geq 0$ and $\operatorname{sign}(b) = -1$ if $b < 0$. Note that if $b = 0$, then a must equal r (and so $\operatorname{arccosh}(\frac{a}{r}) = 0$). This equation is solvable (for either value of $\operatorname{sign}(b)$) if and only if

$$\left(\frac{d}{r} + \sqrt{\frac{d^2}{r^2} - 1} \right) \left(\frac{a}{r} + \sqrt{\frac{a^2}{r^2} - 1} \right) = 1 + \frac{\hat{\delta}^2}{r^2} + \frac{\hat{\delta}}{r} \sqrt{2 + \frac{\hat{\delta}^2}{r^2}}$$

when $b \leq 0$, or

$$\frac{\frac{d}{r} + \sqrt{\frac{d^2}{r^2} - 1}}{\frac{a}{r} + \sqrt{\frac{a^2}{r^2} - 1}} = 1 + \frac{\hat{\delta}^2}{r^2} + \frac{\hat{\delta}}{r} \sqrt{2 + \frac{\hat{\delta}^2}{r^2}}$$

when $b \geq 0$, for some $r \in (0, a]$. The right-hand side of these two equations has the following properties:

- (1) It is a nonincreasing function of $r \in (0, a]$.
- (2) It attains some finite positive value at $r = a$.
- (3) It is greater than the function $2\hat{\delta}^2/r^2$.

- (4) It approaches $2\hat{\delta}^2/r^2$ asymptotically as $r \rightarrow 0$.

The left-hand sides of these two equations have the following properties:

- (1) They attain the same finite positive value at $r = a$.
- (2) The first one is a nonincreasing function of $r \in (0, a]$.
- (3) The second one is a nondecreasing function of $r \in (0, a]$.
- (4) The second one attains the value $\frac{d}{a}$ at $r = 0$.
- (5) The first one is less than the function $4ad/r^2$.
- (6) The first one approaches $4ad/r^2$ asymptotically as $r \rightarrow 0$.

It follows from these properties that one of the two equations above has a solution for some r if and only if $2ad > \hat{\delta}^2$. This completes the proof. \square

We now derive an explicit formula for discrete minimal catenoids, by specifying the vertices along a planar polygonal meridian. Then the traces of the surfaces will have dihedral symmetry of order $k \geq 3$. The surfaces are tessellated by planar isosceles trapezoids like a \mathbb{Z}^2 grid, and each trapezoid can be triangulated into two triangles by choosing a diagonal of the trapezoid as the interior edge. Either diagonal can be chosen, as this does not affect the minimality of the catenoid, by Remark 2.2.

The discrete catenoid has two surprising features. First, the vertices of a meridian lie on a scaled smooth cosh curve (just as the profile curve of smooth catenoids lies on the cosh curve), and there is no a priori reason to have expected this. Secondly, the vertical spacing of the vertices along the meridians is constant.

Theorem 3.1. *There exists a four-parameter family of embedded and complete discrete minimal catenoids $C = C(\theta, \delta, r, z_0)$ with dihedral rotational symmetry and planar meridians. If we assume that the dihedral symmetry axis is the z -axis and that a meridian lies in the xz -plane, then, up to vertical translation, the catenoid is completely described by the following properties:*

- (1) *The dihedral angle is $\theta = \frac{2\pi}{k}$, $k \in \mathbb{N}$, $k \geq 3$.*
- (2) *The vertices of the meridian in the xz -plane interpolate the smooth cosh curve*

$$x(z) = r \cosh\left(\frac{1}{r}az\right),$$

with

$$a = \frac{r}{\delta} \operatorname{arccosh}\left(1 + \frac{1}{r^2} \frac{\delta^2}{1 + \cos\theta}\right),$$

where the parameter $r > 0$ is the waist radius of the interpolated cosh curve, and $\delta > 0$ is the constant vertical distance between adjacent vertices of the meridian.

- (3) *For any given arbitrary initial value $z_0 \in \mathbb{R}$, the profile curve has vertices of the form $(x_j, 0, z_j)$ with*

$$\begin{aligned} z_j &= z_0 + j\delta \\ x_j &= x(z_j) \end{aligned}$$

where $x(z)$ is the meridian in item 2 above.

- (4) *The planar trapezoids of the catenoid may be triangulated independently of each other (by Remark 2.2).*

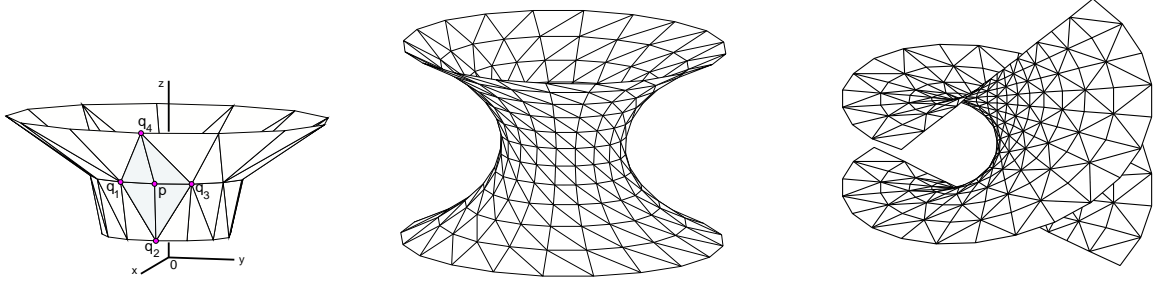


FIGURE 4. The construction in Lemma 3.1, and a discrete minimal catenoid and helicoid. (For this helicoid we have chosen $x_0 = 0$.)

Proof. By Lemma 3.1, if we have three consecutive vertices (x_{n-1}, z_{n-1}) , (x_n, z_n) , and (x_{n+1}, z_{n+1}) along the meridian in the xz -plane which satisfy the recursion formula

$$(10) \quad x_{n+1} = \frac{(x_{n-1} + 2x_n)\hat{\delta}^2 + 2x_n^3}{2x_n x_{n-1} - \hat{\delta}^2}, \quad z_{n+1} = z_n + \delta,$$

where $\delta = z_n - z_{n-1}$ and $\hat{\delta} = \delta/\sqrt{1 + \cos\theta}$. As seen in Lemma 3.1, the vertical distance between (x_{n-1}, z_{n-1}) and (x_n, z_n) is the same as the vertical distance between (x_n, z_n) and (x_{n+1}, z_{n+1}) , so we may consider δ and $\hat{\delta}$ to be constants independent of n .

In order for the surface to exist, Lemma 3.1 requires that

$$2x_n x_{n-1} > \hat{\delta}^2.$$

This implies that all x_n have the same sign, and we may assume $x_n > 0$ for all n . Therefore the surface is embedded. Also, as the condition $2x_n x_{n-1} > \hat{\delta}^2$ implies

$$2x_{n+1} x_n = \frac{2x_n(x_{n-1} + 2x_n)\hat{\delta}^2 + 4x_n^4}{2x_n x_{n-1} - \hat{\delta}^2} > \frac{2x_n x_{n-1} \hat{\delta}^2}{2x_n x_{n-1} - \hat{\delta}^2} > \hat{\delta}^2,$$

we see, inductively, that x_j is defined for all $j \in \mathbb{Z}$. Hence the surface is complete.

One can easily check that the function $x(z)$ in the theorem also satisfies the recursion formula (10), in the sense that if $x_j := x(z_j)$, then these x_j satisfy this recursion formula. It only remains to note that, given two initial points (x_{n-1}, z_{n-1}) and (x_n, z_n) with $z_n > z_{n-1}$, there exists an r so that these two points lie on the curve $x(z)$ with our given δ and θ (up to vertical translation) if and only if $2x_n x_{n-1} > \hat{\delta}^2$, as shown in Lemma 3.2. \square

Remark 3.1. *If we consider the symmetric example with normalized waist radius $r = 1$, that is if we choose $(x_1, z_1) = (1, 0)$ and $(x_2, z_2) = (1 + \hat{\delta}^2, \delta)$, then the recursion formula in Equation (10) implies that*

$$(x_n, z_n) = \left(1 + \sum_{j=1}^{n-1} 2^{j-1} a_{n-1,j} \hat{\delta}^{2j}, (n-1)\delta\right), \quad \text{for } n \geq 3,$$

where $a_{n-1,j}$ is defined recursively by $a_{n,m} = 0$ if $m < 0$ or $n < 0$ or $m > n$, $a_{0,0} = 1$, $a_{n,0} = 2$ if $n > 0$, and $a_{n,m} = 2a_{n-1,m} - a_{n-2,m} + a_{n-1,m-1}$ if $n \geq m \geq 1$.

Thus

$$a_{n,m} = \binom{n+m}{2m} + \binom{n+m-1}{2m}.$$

These $a_{n,m}$ are closely related to the recently solved refined alternating sign matrix conjecture [5].

Corollary 3.1. *There exists a two-parameter family of discrete catenoids $C_1(\theta, z_0)$ whose vertices interpolate the smooth minimal catenoid with meridian $x = \cosh z$.*

Proof. The waist radius of the scaled cosh curve must be $r = 1$. Further, we must choose the parameter $a = 1$ which is fulfilled if θ and δ are related by $1 + \cos \theta + \delta^2 = (1 + \cos \theta) \cosh \delta$. The offset parameter z_0 may be chosen arbitrarily leading to a vertical shift of the vertices along the smooth catenoid. Note that if $z_0 = 0$, we obtain a discrete catenoid that is symmetric with respect to a horizontal reflection. \square

Corollary 3.2. *For each fixed r and z_0 , the profile curves of the discrete catenoids $C(\theta, \delta, r, z_0)$ approach the profile curve $x = r \cosh \frac{z}{r}$ of a smooth catenoid uniformly in compact sets of \mathbb{R}^3 as $\delta, \theta \rightarrow 0$.*

Proof. This is a direct consequence of the explicit representation of the meridian. Since

$$\lim_{\delta \rightarrow 0} \frac{1}{\delta} \operatorname{arccosh}\left(1 + \frac{1}{r^2} \frac{\delta^2}{1 + \cos \theta}\right) = \frac{\sqrt{2}}{r\sqrt{1 + \cos \theta}},$$

it follows that the profile curve of the discrete catenoid converges uniformly to the curve

$$x = r \cosh \frac{\sqrt{2}z}{r\sqrt{1 + \cos \theta}}$$

as $\delta \rightarrow 0$. Then, as $\theta \rightarrow 0$ we approach the profile curve $x = r \cosh \frac{z}{r}$. \square

3.2. Discrete Minimal Helicoids. We continue on to the derivation of explicit discrete helicoids, which are a natural second example of complete, embedded discrete minimal surfaces.

In the smooth setting, there exists an isometric deformation through conjugate surfaces from the catenoid to the helicoid (see, for example, [16]). So, one might first try to make a similar deformation from the discrete catenoids in Theorem 3.1 to discrete minimal helicoids. But such a deformation is impossible in the space of edge-continuous triangulations. In fact, in order to make an associate family of discrete minimal surfaces, one must allow non-continuous triangle nets having greater flexibility, as described in [18].

Therefore, we adopt a different approach for finding discrete minimal helicoids. The helicoids will be comprised of planar quadrilaterals, each triangulated by four coplanar triangles, see Figures 4 and 5. Each quadrilateral is the star of a unique vertex, and none of its four boundary edges are vertical or horizontal, and one pair of opposite vertices in its boundary have the same z -coordinate, and the four boundary edges consist of two pairs of adjacent edges so that within each pair the adjacent edges are of equal length.

First we derive an explicit representation for a particular vertex star to be minimal, as this will help us describe helicoids:

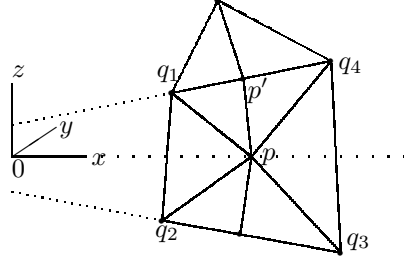


FIGURE 5. $\text{star}(p)$ is the portion considered in Lemma 3.3, and $\text{star}(p')$ is a planar quadrilateral, like the ones comprising the helicoid in Figure 4. Note that the vertex p' can be moved freely inside the planar quadrilateral $\text{star}(p')$ without affecting minimality, by Remark 2.2.

Lemma 3.3. *Let p be a point with a vertex star consisting of four vertices q_1, q_2, q_3, q_4 and four triangles $\Delta_i = (p, q_i, q_{i+1})$, $i \in \{1, 2, 3, 4\} \pmod{4}$. We assume that $p = (u, 0, 0)$, $q_1 = (b \cos \theta, b \sin \theta, 1)$, $q_2 = (b \cos \theta, -b \sin \theta, -1)$, $q_3 = (t \cos \theta, -t \sin \theta, -1)$, $q_4 = (t \cos \theta, t \sin \theta, 1)$ with real numbers $b < u < t$ and $\theta \in (0, \frac{\pi}{2})$. If either*

$$t = -b(1 + 2u^2 \sin^2 \theta) + 2u\sqrt{1 + b^2 \sin^2 \theta}\sqrt{1 + u^2 \sin^2 \theta} \quad \text{or}$$

$$b = -t(1 + 2u^2 \sin^2 \theta) + 2u\sqrt{1 + t^2 \sin^2 \theta}\sqrt{1 + u^2 \sin^2 \theta},$$

then ∇_p area vanishes.

Proof. Consider the conormals $J_1 = J(q_2 - q_1)$, $J_2 = J(q_3 - q_2)$, $J_3 = J(q_4 - q_3)$, $J_4 = J(q_1 - q_4)$, where J denotes oriented rotation by angle $\frac{\pi}{2}$ in the triangle Δ_j containing the edge being rotated. Then

$$J_1 = (2\sqrt{1 + b^2 \sin^2 \theta}, 0, 0) \quad \text{and} \quad J_3 = (-2\sqrt{1 + t^2 \sin^2 \theta}, 0, 0).$$

Since $\langle J_4, (\cos \theta, \sin \theta, 0) \rangle = 0$ and $\det(J_4, (\cos \theta, \sin \theta, 0), (u - b \cos \theta, -b \sin \theta, -1)) = 0$ and $|J_4|^2 = (t - b)^2$, we have that the first component of J_4 (and also of J_2) is

$$\frac{u(t - b) \sin^2 \theta}{\sqrt{1 + u^2 \sin^2 \theta}}.$$

By symmetry, the second and third components of J_2 and J_4 are equal but opposite in sign, hence the second and third components of $J_1 + J_2 + J_3 + J_4$ are zero. So for the minimality condition to hold at p , we need that the first component of $J_1 + J_2 + J_3 + J_4$ is also zero, that is, we need

$$\frac{u(t - b) \sin^2 \theta}{\sqrt{1 + u^2 \sin^2 \theta}} + \sqrt{1 + b^2 \sin^2 \theta} - \sqrt{1 + t^2 \sin^2 \theta} = 0,$$

and the solution of this with respect to b or t is as in the lemma. So, for this solution, ∇_p area vanishes. \square

Theorem 3.2. *There exists a family of complete embedded discrete minimal helicoids, with the connectivity as shown in Figure 4. The vertices, indexed by $i, j \in \mathbb{Z}$, are the points*

$$\frac{r \sinh(x_0 + j\delta)}{\sin \theta} (\cos(i\theta), \sin(i\theta), 0) + (0, 0, ir),$$



FIGURE 6. Discrete analogs of cylinders and Delaunay surfaces.

for any given reals $\theta \in (0, \frac{\pi}{2})$ and $r, \delta \in \mathbb{R}$.

Note that these surfaces are invariant under the screw motion that combines vertical upward translation of distance $2r$ with rotation about the x_3 -axis by an angle of 2θ . The term x_0 determines the offset of the vertices from the z -axis (if $x_0 = 0$, then the z -axis is included in the edge set), and δ determines the horizontal spacing of the vertices. The homothety factor is r , which equals the vertical distance between consecutive horizontal lines of edges.

Proof. Without loss of generality, we may assume $r = 1$. So for a given i , the vertices are points on the line $\{s(\cos(i\theta), \sin(i\theta), i) \mid s \in \mathbb{R}\}$, for certain values of s . We choose x_0 and δ so that the $(j-2)$ 'th vertex has s -value $s_{j-2} = \sinh(x_0 + (j-2)\delta)/\sin\theta$ and the $(j-1)$ 'th vertex has s -value $s_{j-1} = \sinh(x_0 + (j-1)\delta)/\sin\theta$. Lemma 3.3 implies that the j 'th vertex has s -value

$$s_j = -s_{j-2}(1 + 2s_{j-1}^2 \sin^2 \theta) + 2s_{j-1} \sqrt{1 + s_{j-2}^2 \sin^2 \theta} \sqrt{1 + s_{j-1}^2 \sin^2 \theta},$$

a recursion formula that is satisfied by

$$s_j = \sinh(x_0 + j\delta)/\sin\theta.$$

Lemma 3.3 implies a similar formula for determining s_{j-3} in terms of s_{j-2} and s_{j-1} , with the same solution. Finally, noting that those vertices whose star is a planar quadrilateral can be freely moved inside that planar quadrilateral without disturbing minimality of the surface, the theorem is proved. \square

3.3. Discrete Cylinders and Delaunay Surfaces. Here we describe some ways one can find discrete analogs of cylinders and Delaunay surfaces. The strategy for constructing discrete CMC surfaces follows Definition 2.3: position vertices p so that $\nabla_p \text{area}$ is a constant multiple of $\nabla_p \text{vol}$. A simple discrete CMC cylinder is obtained by choosing positive reals a and e and an integer $k \geq 3$, and then choosing the vertices to be

$$p_{j,\ell} = (a \cos(2\pi j/k), a \sin(2\pi j/k), e\ell)$$

for $j, \ell \in \mathbb{Z}$. We then make a grid of rectangular faces, and cut the faces by diagonals with endpoints $p_{j,\ell}$ and $p_{j+1,\ell+1}$. This is a discrete CMC surface with $H = a^{-1}(\cos(\pi/k))^{-1}$. It is interesting to note that H is independent of the value of e . See the left-hand side of Figure 6.

Another special example is to choose positive reals a, b, e , and an integer $k \geq 3$, and to choose the vertices to be

$$p_{j,\ell} = (a \cos(2\pi j/k), a \sin(2\pi j/k), e\ell) \text{ when } j + \ell \text{ is even, and}$$

$$p_{j,\ell} = (b \cos(2\pi j/k), b \sin(2\pi j/k), e\ell) \text{ when } j + \ell \text{ is odd,}$$

for $j, \ell \in \mathbb{Z}$. We then make a grid of quadrilateral faces, and cut the faces by diagonals with endpoints $p_{j,\ell}$ and $p_{j+1,\ell+1}$ if $j + \ell$ is even, and by diagonals with

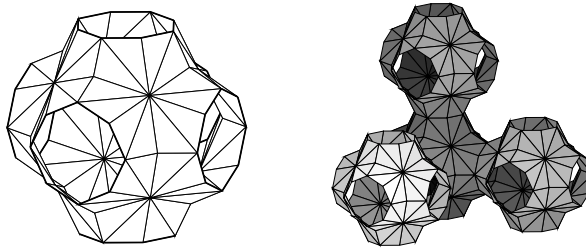


FIGURE 7. A triply-periodic discrete minimal surface with the symmetry of the Schwarz p -surface. Note that one can easily construct surfaces like this with many triangles if the fundamental domains consist of only a few triangles. There is an even simpler example with Schwarz p -surface symmetry whose fundamental piece has only half as many triangles.

endpoints $p_{j,\ell+1}$ and $p_{j+1,\ell}$ if $j + \ell$ is odd. By symmetry, it is clear that $\nabla_{p_{j,\ell}} area$ and $\nabla_{p_{j,\ell}} vol$ are parallel at each vertex; and for each value of e , one can then show the existence of values of a and b so that H is the same value at all vertices, using an intermediate value argument. Thus a discrete CMC cylinder is produced. See the second surface in Figure 6.

A third example can be produced by taking the vertices to be

$$p_{j,\ell} = (a \cos(2\pi j/k), a \sin(2\pi j/k), e\ell) \text{ when } \ell \text{ is even, and}$$

$$p_{j,\ell} = (b \cos(2\pi j/k), b \sin(2\pi j/k), e\ell) \text{ when } \ell \text{ is odd,}$$

for $j, \ell \in \mathbb{Z}$. We then make a grid of isosceles trapezoidal faces, and put an extra vertex in each of the trapezoidal faces, and connect this extra vertex by edges to each of the four vertices of the surrounding trapezoid. Placing the vertices of the surface numerically as symmetric as possible so that Definition 2.3 is satisfied, surfaces like the last two examples in Figure 6 can be produced.

Remark 3.2. *The 2-dimensional boundaries of the tetrahedron, octahedron, and icosahedron are discrete CMC surfaces in our variational characterization, as well as in the sense of [15]. The boundaries of the cube and dodecahedron are not discrete surfaces in our sense, as they are not triangulated. However, by adding a vertex to the center of each face and connecting it by edges to each vertex in the boundary of the face, we can make discrete surfaces, and then we can move these face-centered vertices perpendicularly to the faces to adjust the mean curvature.*

4. JACOBI OPERATOR FOR SMOOTH CMC SURFACES

We now begin the study of the spectra of the second variation of CMC surfaces, and in this section we consider smooth surfaces. In particular, here we explicitly determine the eigenvalues and eigenfunctions of the Jacobi operator for portions of smooth catenoids, which will have applications to section 7. Also, here we state the well-known connection between the second variation and the Jacobi operator in the smooth case, which motivates the computations we do for the discrete case in sections 5 and 6.

Let $\Phi : M \rightarrow \mathbb{R}^3$ be an immersion of a compact 2-dimensional surface M . Let \vec{N} be a unit normal vector field on $\Phi(M)$. Let $\Phi(t)$ be a smooth variation of immersions for $t \in (-\epsilon, \epsilon)$ so that $\Phi(0) = \Phi$ and $\Phi(t)|_{\partial M} = \Phi(0)|_{\partial M}$ for all $t \in (-\epsilon, \epsilon)$. Let

$\vec{U}(t)$ be the variation vector field on $\Phi(t)$. We can assume, by reparametrizing $\Phi(t)$ for nonzero t if necessary, that the corresponding variation vector field at $t = 0$ is $\vec{U}(0) = u\vec{N}$, with $u \in C^\infty(M)$ and $u|_{\partial M} = 0$. Let $a(t)$ be the area of $\Phi(t)(M)$ and H be the mean curvature of $\Phi(M)$. The first variational formula is

$$a'(0) := \left. \frac{d}{dt} a(t) \right|_{t=0} = - \int_M \langle nH\vec{N}, u\vec{N} \rangle dA,$$

where \langle, \rangle and dA are the metric and area form on M induced by the immersion Φ . We now assume H is constant, so $a'(0) = -nH \int_M u dA$. Let $V(t)$ be the volume of $\Phi(t)(M)$, then $V'(0) = \int_M u dA$. The variation is *volume preserving* if $\int_M \langle \vec{U}(t), \vec{N}(t) \rangle dA(t) = 0$ for all $t \in (-\epsilon, \epsilon)$. In particular, $\int_M u dA = 0$ when $t = 0$, so $a'(0) = 0$ and $\Phi(M)$ is critical for area amongst all volume preserving variations.

The second variation formula for volume preserving variations $\Phi(t)$ is

$$a''(0) := \left. \frac{d^2}{dt^2} a(t) \right|_{t=0} = \int_M \{ |\nabla u|^2 - (4H^2 - 2K)u^2 \} dA = \int_M uLu dA,$$

where K is the Gaussian curvature on M induced by Φ , and

$$(11) \quad L = -\Delta - 4H^2 + 2K$$

is the Jacobi operator with Laplace-Beltrami operator Δ .

There are two ways that the index of a smooth CMC surface can be defined: the geometric definition for $\text{Ind}(M) = \text{Ind}(\Phi(M))$ is the maximum possible dimension of a subspace \mathcal{S} of volume-preserving variation functions $u \in C_0^\infty(M)$ for which $a''(0) < 0$ for all nonzero $u \in \mathcal{S}$. The analytic definition for $\text{Ind}_U(M)$ is the number of negative eigenvalues of the operator L , which equals the maximum possible dimension of a subspace \mathcal{S}_U of (not necessarily volume-preserving) variation functions $u \in C_0^\infty(M)$ for which $\int_M uLu dA < 0$ for all nonzero $u \in \mathcal{S}_U$. The subscript U stands for “Unconstrained index”.

We have $\text{Ind}_U(M) \geq \text{Ind}(M) \geq \text{Ind}_U(M) - 1$, see [10]. As it is geometrically more natural, we want to compute $\text{Ind}(M)$. But $\text{Ind}_U(M)$ is more accessible to computation than $\text{Ind}(M)$, and they differ only by at most 1.

In the case that we are considering minimal surfaces, as in section 7, the volume constraint is not necessary, and hence $\text{Ind}(M) = \text{Ind}_U(M)$.

4.1. Eigenvectors of L for Rectangles. Consider the minimal rectangle

$$M = \{(x, y, 0) \in \mathbb{R}^3 \mid 0 \leq x \leq x_0, 0 \leq y \leq y_0\}$$

with natural coordinates $(x, y) \in \mathbb{R}^2$, and consider functions on M with Dirichlet boundary conditions. Then $L = -\Delta$ with eigenvalues and eigenfunctions

$$\lambda_{m,n} = \frac{m^2\pi^2}{x_0^2} + \frac{n^2\pi^2}{y_0^2}, \quad \phi_{m,n} = \frac{2}{\sqrt{x_0 y_0}} \sin \frac{m\pi x}{x_0} \sin \frac{n\pi y}{y_0}$$

for $(m, n) \in \mathbb{Z}^+ \times \mathbb{Z}^+$. Hence $\text{Ind}(M) = 0$.

4.2. Eigenvectors of L for Catenoids. The catenoid is given as a conformal map

$$\Phi : (x, y) \in \mathcal{R} \rightarrow (\cos x \cosh y, \sin x \cosh y, y) \in \mathbb{R}^3,$$

with $\mathcal{R} = S^1 \times [y_0, y_1]$. The metric, Laplace-Beltrami operator, and Gauss curvature are

$$ds^2 = \cosh^2 y \cdot (dx^2 + dy^2), \quad \Delta = \frac{\partial^2}{\partial^2 x} + \frac{\partial^2}{\partial^2 y}, \quad K = -\cosh^{-4} y.$$

We put Dirichlet boundary conditions on the two boundary curves of \mathcal{R} .

Lemma 4.1. *The catenoid Φ has an L^2 -basis of eigenfunctions for its Jacobi operator $L = -\Delta + 2K$ of the form $\sin(mx)f(y)$ or $\cos(mx)f(y)$, for $m \in \mathbb{N} \cup \{0\}$. The function f is a solution of the 2nd-order ordinary differential equation*

$$(12) \quad f_{yy} = (m^2 - \lambda \cosh^2 y - 2 \cosh^{-2} y) f,$$

with eigenvalue $\lambda \in \mathbb{R}$ of L and Dirichlet boundary conditions $f(y_0) = f(y_1) = 0$.

Therefore, the eigenvalues λ and eigenfunctions of L are determined by the solutions of Equation (12) with $f(y_0) = f(y_1) = 0$.

Proof. It is well known that L , with respect to the Dirichlet boundary condition, has a discrete spectrum in \mathbb{R} , and that, for all $\lambda \in \mathbb{R}$, $\ker(L - \lambda)$ is a finite dimensional space of smooth functions. Furthermore, an orthonormal basis of the L^2 space over \mathcal{R} (with respect to ds^2) can be obtained as a set of smooth eigenfunctions of L satisfying the Dirichlet boundary condition.

Define the symmetric operator $D = i \frac{\partial}{\partial x}$. To see that D is symmetric, for functions u and v that are 2π -periodic in x we have

$$\left\langle \frac{\partial}{\partial x} u, v \right\rangle_{L^2} + \left\langle u, \frac{\partial}{\partial x} v \right\rangle_{L^2} = \int_{\mathcal{R}} (u_x \bar{v} + u \bar{v}_x) \cosh^2 y dx dy = 0,$$

which implies that the operator $\frac{\partial}{\partial x}$ is skew symmetric, and so D is symmetric.

Note that $DL = LD$, so $D : \ker(L - \lambda) \rightarrow \ker(L - \lambda)$. Since D is symmetric, it has a basis of eigenfunctions in each finite dimensional space $\ker(L - \lambda)$. So we can choose a set of functions that is simultaneously an L^2 -basis of eigenfunctions for both D and L . Since the eigenfunctions of D must be of the form $e^{mxi} f(y)$ with $m \in \mathbb{Z}$, the first part of the lemma follows.

An eigenfunction $\sin(mx)f(y)$ of L satisfies

$$\begin{aligned} L(\sin(mx)f(y)) &= \lambda \sin(mx)f(y) \\ &= \frac{m^2 \sin(mx)f(y)}{\cosh^2 y} - \frac{\sin(mx)f_{yy}(y)}{\cosh^2 y} - \frac{2 \sin(mx)f(y)}{\cosh^4 y}, \end{aligned}$$

and a similar computation holds for an eigenfunction $\cos(mx)f(y)$. Hence f satisfies Equation (12). \square

5. SECOND VARIATION OF AREA

We now consider the spectra of the second variation for discrete CMC surfaces $\mathcal{T}(t)$ as in Definition 2.2, and we begin with a technical and explicit computation of the second variation in this section.

Lemma 5.1. *For a compact discrete CMC H surface \mathcal{T} with vertex set \mathcal{V} ,*

$$\left. \frac{d^2}{dt^2} \text{area}(\mathcal{T}) \right|_{t=0} = \sum_{p \in \mathcal{V}} \langle p', (\nabla_p \text{area})' - H(\nabla_p \text{vol})' \rangle$$

for any permissible variation.

Proof. Differentiating Equation (2) and using Definition 2.3, we have

$$(\text{area})''(0) = \sum_{p \in \mathcal{V}} \langle p'', H \nabla_p \text{vol} \rangle + \sum_{p \in \mathcal{V}} \langle p', (\nabla_p \text{area})' \rangle.$$

For a minimal discrete surface, the first term on the right hand side vanishes. For a discrete CMC surface with $H \neq 0$, the variation $p(t)$ is volume preserving for all t , so by Equation (4) we have

$$\sum_{p \in \mathcal{V}} \langle p', \nabla_p \text{vol} \rangle = 0 \quad \forall t \implies \sum_{p \in \mathcal{V}} \langle p'', \nabla_p \text{vol} \rangle + \langle p', (\nabla_p \text{vol})' \rangle = 0,$$

proving the lemma. \square

Definition 5.1. *A discrete minimal or CMC surface \mathcal{T} is stable if $(\text{area})''(0) \geq 0$ for any permissible (i.e. volume-preserving and boundary-fixing) variation.*

For any permissible variation as in Equation (5) with $\vec{v} \in \mathbb{R}^{3n}$ as in Equation (6), the second variation $(\text{area})''(0)$ is a bilinear form which can be represented by a symmetric $3n \times 3n$ matrix Q , so that $\vec{v}^t Q \vec{v}$ equals $(\text{area})''(0)$. We now decompose $(\text{area})''(0)$ into the sum of two terms

$$(13) \quad \vec{v}^t Q^a \vec{v} := \sum_{p \in \mathcal{V}} \langle v_p, (\nabla_p \text{area})' \rangle \quad \text{and} \quad -H \vec{v}^t Q^V \vec{v} := -H \sum_{p \in \mathcal{V}} \langle v_p, (\nabla_p \text{vol})' \rangle,$$

for any permissible variation with variation vector field \vec{v} . In the next two propositions we determine the components of the matrices Q^a and Q^V satisfying Equation (13), thus giving us the components of $Q = Q^a - H Q^V$.

Proposition 5.1. *The hessian of the area function from S_h to \mathbb{R} is a symmetric bilinear form with $3n \times 3n$ matrix representation Q^a , with respect to the basis $\{\psi_{p_j}\}$ of S_h . Q^a can be considered as an $n \times n$ grid with a 3×3 entry $Q_{i,j}^a$ for each pair of interior vertices $p_i, p_j \in \mathcal{V}_{int}$ of \mathcal{T} , so that*

$$\vec{v}^t Q^a \vec{v} = \sum_{p \in \mathcal{V}} \langle v_p, (\nabla_p \text{area})' \rangle$$

for the variation vector field \vec{v} of any permissible variation. The entry $Q_{i,j}^a$ is 0 if the vertices p_i, p_j are not adjacent, and is

$$Q_{i,j}^a = \frac{1}{2} \sum_{\substack{T=(p_i, p_j, r) \in \text{star}(p_i p_j), \\ \vec{e}_{ij} := p_i - p_j}} \frac{\vec{e}_{ij} \cdot J^t(\vec{e}_{ij}) - J(\vec{e}_{ij}) \cdot \vec{e}_{ij}^t}{|\vec{e}_{ij}|^2} - \cot \theta_T \vec{N}_T \cdot \vec{N}_T^t$$

for p_i and p_j adjacent and unequal, where θ_T is the interior angle of the triangle $T = (p_i, p_j, r)$ at r , and is

$$Q_{i,i}^a = \frac{1}{4} \sum_{T=(p_i, q, r) \in \text{star}(p_i)} \frac{|r - q|^2}{\text{area } T} \vec{N}_T \vec{N}_T^t$$

when the vertices are both equal to p_i . Here, \vec{N}_T (or just \vec{N}) denotes the oriented unit normal vector of the triangle $T = (p, q, r)$.

Proposition 5.2. *The hessian of the volume function from S_h to \mathbb{R} is a symmetric bilinear form with $3n \times 3n$ matrix representation Q^V , with respect to the basis $\{\psi_{p_j}\}$ of S_h . Q^V has a 3×3 entry $Q_{i,j}^V$ for each pair of vertices $p_i, p_j \in \mathcal{V}_{int}$ of \mathcal{T} , so that*

$$\vec{v}^t Q^V \vec{v} = \sum_{p \in \mathcal{V}} \langle v_p, (\nabla_p \text{vol})' \rangle$$

for the variation vector field \vec{v} of any permissible variation. We have $Q_{i,i}^V = 0$, and $Q_{i,j}^V = 0$ when the vertices p_i and p_j are not adjacent, and

$$Q_{i,j}^V = \frac{1}{6} \begin{pmatrix} 0 & r_{2,3} - r_{1,3} & r_{1,2} - r_{2,2} \\ r_{1,3} - r_{2,3} & 0 & r_{2,1} - r_{1,1} \\ r_{2,2} - r_{1,2} & r_{1,1} - r_{2,1} & 0 \end{pmatrix}$$

for adjacent unequal p_i and p_j , where (p_i, p_j, r_k) are the two triangles in $\text{star}(\overline{p_i p_j})$ and $r_k = (r_{k,1}, r_{k,2}, r_{k,3})$ for $k = 1, 2$, and (p_i, p_j, r_2) is properly oriented and (p_i, p_j, r_1) is not.

The proofs of these two propositions are technical computations, so we give them in an appendix to this paper.

Corollary 5.1. *If a discrete CMC surface \mathcal{T} has only one interior vertex, then it is stable.*

Proof. The single interior vertex is denoted by p_1 , and $\text{star}(p_1) = \mathcal{T}$. Then $Q^a = Q_{1,1}^a$ and $Q^V = Q_{1,1}^V$ are 3×3 matrices. By Propositions 5.1 and 5.2, $Q^V = 0$ and for any vector $u_p \in \mathbb{R}^3$ at p we have that $u_p^t Q^a u_p$ equals

$$\frac{1}{4} \sum_{T=(p,q,r) \in \mathcal{T}} \frac{|r-q|^2}{\text{area } T} u_p^t \vec{N} \vec{N}^t u_p = \frac{1}{4} \sum_{T=(p,q,r) \in \mathcal{T}} \frac{|r-q|^2}{\text{area } T} \langle u_p, \vec{N} \rangle^2 \geq 0,$$

so $(\text{area})''(0) \geq 0$ for all permissible variations. \square

6. JACOBI OPERATOR FOR DISCRETE CMC SURFACES

Since we know the second variation matrix Q explicitly (section 5), we are now able to find the discrete Jacobi operator for compact discrete CMC surfaces \mathcal{T} , analogous to L in the smooth case (see Equation (11)). In this section, we find the correct matrix for the discrete Jacobi operator; this matrix has the eigenvalues and eigenfunctions of the second variation of \mathcal{T} .

We begin with an explicit form for the L^2 inner product on S_h with respect to the basis $\{\psi_{p_1}, \dots, \psi_{p_n}\}$:

Lemma 6.1. *The L^2 norm*

$$\langle u, v \rangle_{L^2} := \int_{\mathcal{T}} \langle u, v \rangle dA = \sum_{T \subset \mathcal{T}} \int_T \langle u|_T, v|_T \rangle dA$$

on \mathcal{T} for $u, v \in S_h$ has the positive definite $3n \times 3n$ matrix representation

$$S = (\langle \psi_{p_i}, \psi_{p_j} \rangle_{L^2} I_{3 \times 3})_{i,j=1}^n,$$

so that $\langle u, v \rangle_{L^2} = \vec{u}^t S \vec{v}$, where $\vec{u}, \vec{v} \in \mathbb{R}^{3n}$ are the vector fields associated to u, v . S consists of 3×3 blocks $S_{i,j}$ in an $n \times n$ grid with

$$S_{j,j} = \sum_{T \in \text{star}(p_j)} \frac{\text{area } T}{6} \cdot I_{3 \times 3}, \quad \text{resp. } S_{i,j} = \sum_{T \in \text{star}(\overline{p_i p_j})} \frac{\text{area } T}{12} \cdot I_{3 \times 3}$$

when p_i and p_j are adjacent, and $S_{i,j} = 0$ when p_i and p_j are not adjacent.

Proof. Noting that, for each triangle $T \subset \mathcal{T}$,

$$\int_T \psi_p^2 dA = \frac{\text{area } T}{6}, \quad \int_T \psi_p \psi_q dA = \frac{\text{area } T}{12}$$

for any distinct vertices p and q of T , and using Equation (7), we have that, for any two functions $u, v \in S_h$, $\langle u, v \rangle_{L^2}$ equals

$$\sum_{p_j \in \mathcal{V}_{int}} \left(\langle u_{p_j}, v_{p_j} \rangle \sum_{T \in \text{star}(p_j)} \frac{\text{area } T}{6} + \sum_{\substack{p_i \in \mathcal{V}_{int} \\ \text{adjacent to } p_j}} \langle u_{p_j}, v_{p_i} \rangle \sum_{T \in \text{star}(\overline{p_i p_j})} \frac{\text{area } T}{12} \right).$$

Hence the 3×3 blocks $S_{i,j}$ are as in the lemma. \square

We now define the discrete Jacobi operator $L_h : S_h \rightarrow S_h$ associated to the second variation formula for the surface (recall Equations (5), (6), and (7)).

Definition 6.1. For $v \in S_h$ with associated vector field \vec{v} , we define the discrete Jacobi operator $L_h v$ on v to be the function in S_h associated to the vector field $S^{-1}Q\vec{v}$.

$L_h(S_h) \subset S_h$, so we can consider the eigenvalue problem for L_h . We also desire L_h to be linear and symmetric ($\int_{\mathcal{T}} u^t L_h v = \int_{\mathcal{T}} v^t L_h u$ for all $u, v \in S_h$). With these properties, the above choice of L_h is canonical:

Proposition 6.1. $L_h : S_h \rightarrow S_h$ is the unique linear operator so that $\int_{\mathcal{T}} u^t L_h v dA$ is symmetric in u and v and

$$\int_{\mathcal{T}} v^t L_h v dA = \vec{v}^t Q \vec{v}$$

for all $v \in S_h$.

Proof. The map L_h is clearly linear, and

$$\int_{\mathcal{T}} u^t L_h v dA = \langle u, L_h v \rangle_{L^2} = \vec{u}^t S(S^{-1}Q\vec{v}) = \vec{u}^t Q \vec{v}$$

for all $u, v \in S_h$. Hence, since Q is symmetric, $\int_{\mathcal{T}} u^t L_h v dA$ is symmetric in u and v .

Uniqueness of L_h with the above properties follows from the following:

$$\begin{aligned} \int_{\mathcal{T}} u^t L_h v dA &= \frac{1}{2} \left(\int_{\mathcal{T}} (u+v)^t L_h (u+v) dA - \int_{\mathcal{T}} u^t L_h u dA - \int_{\mathcal{T}} v^t L_h v dA \right) \\ &= \frac{1}{2} \left((\vec{u} + \vec{v})^t Q (\vec{u} + \vec{v}) - \vec{u}^t Q \vec{u} - \vec{v}^t Q \vec{v} \right). \end{aligned}$$

Hence $\int_{\mathcal{T}} u^t L_h v dA$ is uniquely determined for all $u \in S_h$, so $L_h v$ is uniquely determined for each $v \in S_h$. \square

Since $S^{-1}Q$ is self-adjoint with respect to the L^2 inner product on S_h , all the eigenvalues of $S^{-1}Q$ are real.

Definition 6.2. The spectrum of the second variation of $\mathcal{T}(t)$ at $t = 0$ is the set of eigenvalues of $S^{-1}Q$.

Remark 6.1. *Another way to see that $S^{-1}Q$ is the correct discrete Jacobi operator is to consider the Rayleigh quotient*

$$\frac{\vec{v}^t Q \vec{v}}{\langle v, v \rangle_{L^2}} = \frac{\vec{v}^t S(S^{-1}Q\vec{v})}{\vec{v}^t S\vec{v}}.$$

The standard minmax procedure for producing eigenvalues from the Rayleigh quotient will produce the eigenvalues of $S^{-1}Q$.

7. APPROXIMATING SPECTRA OF SMOOTH CMC SURFACES

Using our explicit form for $S^{-1}Q$ of the discrete Jacobi operator L_h , we can now implement the procedure described in the second half of the introduction.

If a sequence of compact CMC discrete surfaces $\{\mathcal{T}\}_{i=1}^{\infty}$ converges (in the Sobolev H^1 norm as graphs over the limiting surface) to a smooth compact CMC surface $\Phi : M \rightarrow \mathbb{R}^3$, then standard estimates from the theory of finite elements (see, for example, [4] or [8]) imply that the eigenvalues and eigenvectors (piece-wise linearly extended to functions) of the operators L_h of the \mathcal{T}_j converge to the eigenvalues and eigenfunctions of the Jacobi operator L of Φ (convergence is in the L^2 norm for the eigenfunctions).

For the first two examples here – a planar square and rotationally symmetric portion of a catenoid – we know the approximating discrete minimal surfaces exactly, and we know the eigenvalues and eigenfunctions of L for the smooth minimal surfaces exactly, so we can check that convergence of the eigenvalues and eigenfunctions does indeed occur.

In the final two examples – symmetric portions of a trinoid and a Costa surface – the spectra of the smooth minimal surfaces is unknown, so we see estimates for the eigenvalues and eigenfunctions for the first time. Our experiments confirm the known values 3 and 5 respectively for the indexes of these unstable surfaces, and additionally show us the directions of variations that reduce area. Thus we have approximations for maximal spaces of variation vector fields on the smooth minimal surfaces for which the associated variations reduce area. (For the approximating discrete surfaces in these examples, we do not have an explicit form; however, the theory of finite elements applies and we can still expect convergence of the eigenvalues and eigenfunctions in L^2 norm, if we choose the discrete approximations so that they converge in H^1 norm to the smooth minimal surfaces.)

7.1. The flat minimal square. Considering the square $M = \{0 \leq x \leq \pi, 0 \leq y \leq \pi\}$ included in \mathbb{R}^3 as a smooth minimal surface, the eigenvalues and eigenfunctions of L are $\mu_{m,n} = m^2 + n^2$ and $\phi_{m,n} = \frac{2}{\pi} \sin(mx) \sin(ny)$ for $m, n \in \mathbb{Z}^+$ (section 4).

Now we consider the discrete minimal surface \mathcal{T} that is M with a regular square $n \times n$ grid. In each subsquare of dimension $\frac{\pi}{n} \times \frac{\pi}{n}$, we draw an edge from the lower left corner to the upper right corner, producing a discrete minimal surface with $2n^2$ congruent triangles with angles $\frac{\pi}{4}$, $\frac{\pi}{4}$, and $\frac{\pi}{2}$.

For this \mathcal{T} , $S^{-1}Q$ has no negative eigenvalues, as expected, since the smooth minimal square is stable. However, we must take tangential motions into account in the discrete case, and we find that (when writing the eigenvalues in increasing order) the first two-thirds of the eigenvalues are 0 and their associated eigenvectors are entirely tangent to the surface. The final one-third of the eigenvalues are positive, with eigenvectors that are exactly perpendicular to the surface. Examples of these perpendicular vector fields are shown in Figure 8 for $n = 15$. (There are 196 interior

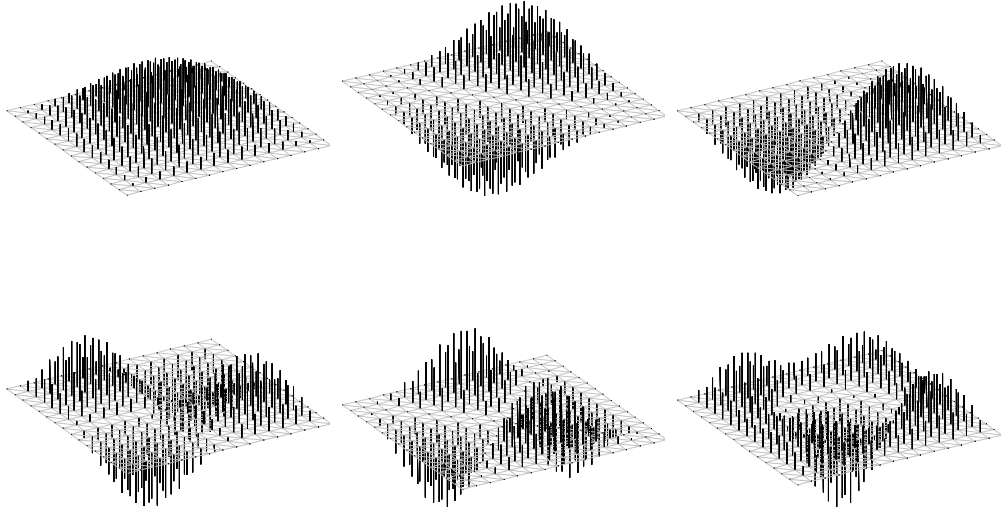


FIGURE 8. The eigenvectors of the discrete square with $n = 15$ associated to the first six positive eigenvalues described in section 7.1. Note that these eigenvectors closely resemble linear combinations of eigenfunctions of the Laplacian on the smooth square in section 4.1, for example the first two resemble $\sin(x) \sin(y)$ and $\sin(x) \sin(2y) - \sin(2x) \sin(y)$ and the last resembles $\sin(3x) \sin(y) + \sin(x) \sin(3y)$.

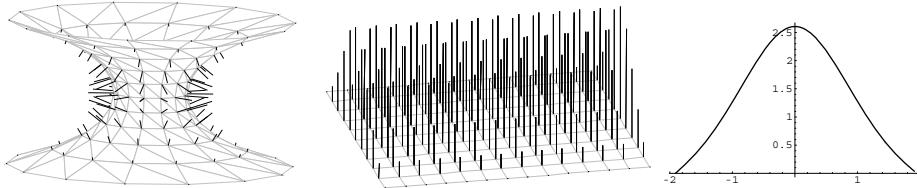


FIGURE 9. On the left is the eigenvector associated to the negative eigenvalue $\lambda_0 \approx -0.542$ of an unstable discrete catenoid. In the middle we have also shown this \mathbb{R}^{3n} -vector field on the domain grid (where each \mathbb{R}^3 -vector is vertical with length equal to that of the corresponding \mathbb{R}^3 -vector in the \mathbb{R}^{3n} -eigenvector field on the discrete catenoid), to show the close resemblance to the eigenfunction on the right for the smooth case. The function $f(y)$ (computed numerically) on the right is the eigenfunction when $m = 0$ for the catenoid $\Phi(\mathcal{R})$ in Section 4 with $y_1 = -y_0 = 1.91$. The corresponding eigenvalue is $\lambda \approx -0.54$, and all other eigenvalues are positive.

vertices, and so there are 588 eigenvalues λ_j of $S^{-1}Q$ and $\lambda_0 = \dots = \lambda_{391} = 0$ and $\lambda_j > 0$ when $j \in [392, 587]$.) The eigenvectors shown in these figures and their eigenvalues are close to those of the smooth operator L of M . We have $\lambda_{392} = 2.022 \approx \mu_{1,1}$, $\lambda_{393} = 5.094 \approx \mu_{1,2}$, $\lambda_{394} = 5.148 \approx \mu_{2,1}$, $\lambda_{395} = 8.347 \approx \mu_{2,2}$, $\lambda_{396} = 10.434 \approx \mu_{1,3}$, $\lambda_{397} = 10.445 \approx \mu_{3,1}$.

7.2. Discrete minimal catenoids. By Corollary 3.2, we know that the discrete minimal catenoids converge to smooth catenoids as the meshes are made finer.

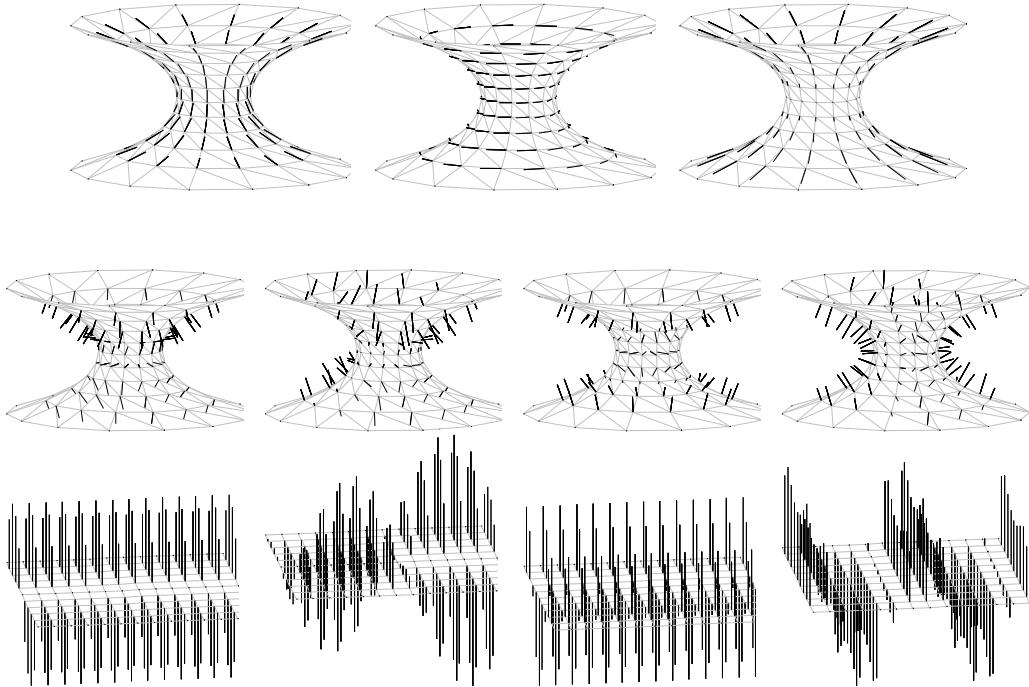


FIGURE 10. Two-thirds of the eigenvectors are approximately tangential to the surface. For example, in the first row we show the \mathbb{R}^{3n} -eigenvector fields associated to the eigenvalues λ_1 , λ_2 , and λ_3 (whose values are just slightly greater than 0). One-third of the eigenvectors are approximately perpendicular to the surface, and the second row shows such eigenvector fields, associated to the eigenvalues λ_{147} , λ_{171} , λ_{204} , and λ_{210} . The final row shows projected versions of the eigenvectors in the second row, for use in comparing with the eigenfunctions of the smooth case considered in section 4. These projected versions are made just as in Figure 9.

Hence the eigenvalues and eigenvectors of the discrete catenoids converge to the eigenvalues and eigenfunctions of the smooth catenoid. For the discrete catenoids with relatively fine meshes, we find that two-thirds of the eigenvectors are approximately tangential to the surface, and the remaining ones are approximately perpendicular. The approximately perpendicular ones (considered as functions which are multiplied by unit normal vectors) and their eigenvalues converge to the eigenfunctions and eigenvalues of the smooth catenoid (computed in section 4).

Consider the example shown in the Figures 9 and 10. Here the catenoid has $9 \times 14 = 126$ interior vertices, so the matrix $S^{-1}Q$ has dimension 378×378 . The first eigenvalue of this matrix is $\lambda_0 \approx -0.542$ and $\lambda_j > 0$ for all $j \in [1, 377]$, as expected, since the smooth complete catenoid has index 1 ([7]). Note that λ_0 is very close to the negative eigenvalue for the smooth case, described in the caption of Figure 9 (the closest matching smooth catenoid portion satisfies $y_1 = -y_0 = 1.91$). The first eigenfunction in the discrete case (also Figure 9) is also very close to the first eigenfunction in the smooth case.

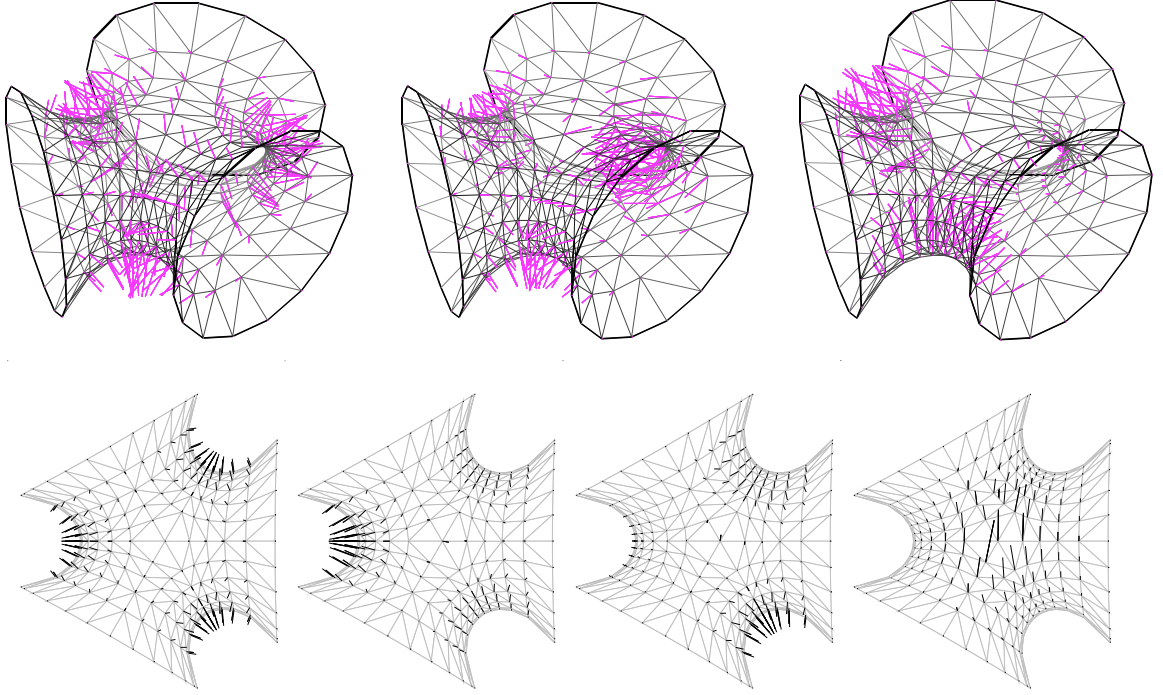


FIGURE 11. Variation vector fields for three area-reducing variations of a discrete approximation of a compact portion of a trinoid. The lower row has overhead views of these variation vector fields, as well as an overhead view of the variation vector field associated to the fourth (and first positive) eigenvalue.

7.3. Discrete minimal trinoids and Costa surfaces. Since the trinoid has index 3, we find that approximating discrete surfaces with relatively fine meshes have 3 negative eigenvalues. And we can look at the corresponding eigenvector fields (which estimate the eigenfunctions in the smooth case), shown in Figure 11. For the approximating discrete trinoid in Figure 11, the first four eigenvalues are approximately $-3.79, -1.31, -1.31, 0.014$, so we indeed have 3 negative eigenvalues and the second eigenvalue has multiplicity 2.

Similarly, the genus 1 Costa surface has index 5, and approximating discrete surfaces with relatively fine meshes have 5 negative eigenvalues. See Figure 12.

APPENDIX A

Here we give the proofs of Propositions 5.1 and 5.2. For notating area and volume, we shall now frequently use "a" and "V" instead of "area" and "vol", for brevity. We will also use $|T|$ or $|(p, q, r)|$ to signify the area of a triangle $T = (p, q, r)$.

Proof. (of Proposition 5.1) If \vec{v} and \vec{w} are variation vector fields for any pair of permissible variations, we can define a bilinear form $Q^a(\vec{v}, \vec{w}) :=$

$$\frac{1}{2} \sum_{T=(p,q,r) \in \mathcal{T}} -\langle v_p \times w_r - v_r \times w_p + v_q \times w_p - v_p \times w_q + v_r \times w_q - v_q \times w_r, \vec{N} \rangle +$$

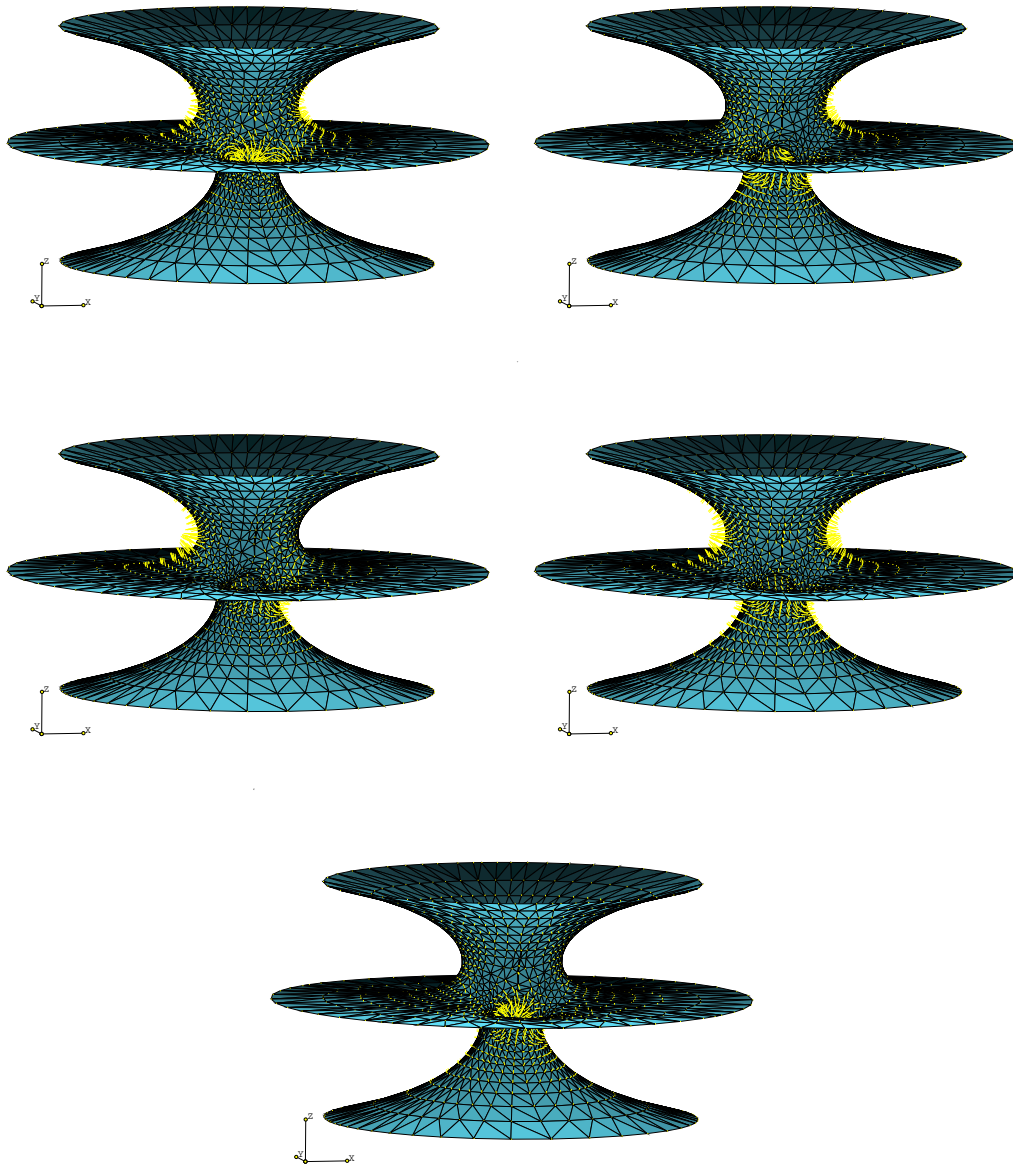


FIGURE 12. The first five eigenvector fields (whose corresponding eigenvalues are the five negative ones) for a discrete approximation of a compact portion of a genus 1 Costa surface.

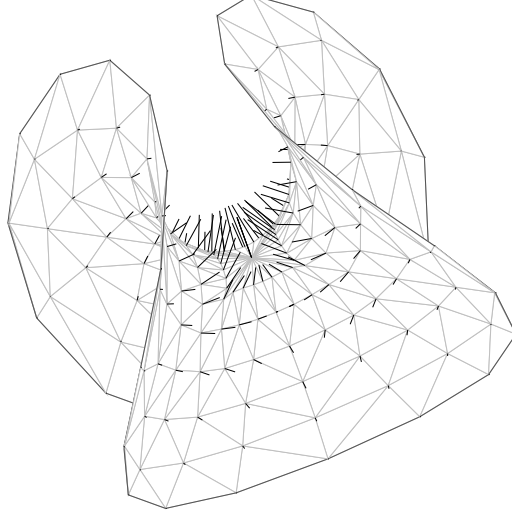


FIGURE 13. The first eigenvector field for a discrete approximation of a compact portion of an Enneper surface. The associated first eigenvalue is negative and is the only negative eigenvalue that is not approximately zero, corresponding to the fact that the smooth Enneper surface has index 1. Those other negative (approximately zero) eigenvalues have corresponding eigenvector fields that appear roughly tangent to the surface.

$$\begin{aligned} & \frac{1}{2|T|} \langle v_p \times (r - q) + v_q \times (p - r) + v_r \times (q - p), \\ & w_p \times (r - q) + w_q \times (p - r) + w_r \times (q - p) \rangle - \\ & \frac{1}{2|T|} \langle v_p \times (r - q) + v_q \times (p - r) + v_r \times (q - p), \vec{N} \rangle \cdot \\ & \langle w_p \times (r - q) + w_q \times (p - r) + w_r \times (q - p), \vec{N} \rangle. \end{aligned}$$

Using $\vec{N}' = \frac{(q-p) \times (r'-p') + (q'-p') \times (r-p)}{2|T|} - \frac{\vec{N}}{2|T|} \langle (q-p) \times (r'-p') + (q'-p') \times (r-p), \vec{N} \rangle$, it follows that $Q^a(\vec{v}, \vec{v}) = \sum_{p \in \mathcal{V}} \langle v_p, (\nabla_p a)' \rangle$. Q^a is clearly bilinear, and the last two terms of Q^a are obviously symmetric in \vec{v} and \vec{w} . The first term is also symmetric in \vec{v} and \vec{w} , since $v_p \times w_r - v_r \times w_p = w_p \times v_r - w_r \times v_p$, $v_q \times w_p - v_p \times w_q = w_q \times v_p - w_p \times v_q$, and $v_r \times w_q - v_q \times w_r = w_r \times v_q - w_q \times v_r$.

It only remains to determine an explicit form for Q^a . For a given interior vertex p , suppose \vec{v} and \vec{w} are nonzero only at p , that is, that $\vec{v}^t = (0^t, \dots, 0^t, v_p^t, 0^t, \dots, 0^t)$ and $\vec{w}^t = (0^t, \dots, 0^t, w_p^t, 0^t, \dots, 0^t)$. Then

$$\begin{aligned} Q^a(\vec{v}, \vec{w}) &= Q_{pp}^a(v_p, w_p) = \frac{1}{4} \sum_{T=(p,q,r) \in \text{star}(p)} \\ & \frac{1}{|T|} \langle v_p \times (r - q), w_p \times (r - q) \rangle - \frac{1}{|T|} \langle v_p \times (r - q), \vec{N} \rangle \langle w_p \times (r - q), \vec{N} \rangle \\ &= \frac{1}{4} \sum_{T=(p,q,r) \in \text{star}(p)} \frac{1}{|T|} v_p^t (|r - q|^2 I - (r - q)(r - q)^t - ((r - q) \times \vec{N})((r - q) \times \vec{N})^t) w_p \\ &= \frac{1}{4} \sum_{T=(p,q,r) \in \text{star}(p)} \frac{|r - q|^2}{|T|} v_p^t (\vec{N} \vec{N}^t) w_p, \end{aligned}$$

hence Q_{pp}^a is of the form in the proposition.

Now suppose $\vec{v}^t = (0^t, \dots, 0^t, v_p^t, 0^t, \dots, 0^t)$ and $\vec{w}^t = (0^t, \dots, 0^t, w_q^t, 0^t, \dots, 0^t)$ for some given unequal interior vertices p and q . If p and q are not connected by some edge of the surface, then clearly $Q^a(\vec{v}, \vec{w}) = 0$, so assume that p and q are adjacent. Note that $\text{star}(\overline{pq})$ then contains two triangles (p, q, r_j) for $j = 1, 2$ and precisely one of them is properly oriented. Noting also that the normal vector \vec{N} of a triangle changes sign when the orientation of the triangle is reversed, we have the following equation:

$$\begin{aligned} Q^a(\vec{v}, \vec{w}) &= Q_{pq}^a(v_p, w_q) = \frac{1}{2} \sum_{T=(p,q,r_k), k=1,2} \langle v_p \times w_q, \vec{N} \rangle + \\ &= \frac{1}{2|T|} \langle v_p \times (r_k - q), w_q \times (p - r_k) \rangle - \frac{1}{2|T|} \langle v_p \times (r_k - q), \vec{N} \rangle \langle w_q \times (p - r_k), \vec{N} \rangle = \\ &= \frac{1}{4} \sum_{k=1}^2 \frac{1}{|T|} v_p^t \left((p - r_k)(q - r_k)^t - (q - r_k)(p - r_k)^t - \langle p - r_k, q - r_k \rangle \vec{N} \vec{N}^t \right) w_q. \end{aligned}$$

For a triangle (p, q, r) , one can check that

$$(p - r)(q - r)^t - (q - r)(p - r)^t = \frac{2|(p, q, r)|}{|p - q|^2} \left((p - q)(J(p - q))^t - J(p - q)(p - q)^t \right),$$

so Q_{pq}^a is as in the proposition. \square

Proof. (of Proposition 5.2) $\sum_{p \in \mathcal{V}} \langle p', (\nabla_p V)' \rangle = \sum_{p \in \mathcal{V}_{int}} \langle v_p, \frac{1}{6} \sum_{(p,q,r) \in \text{star}(p)} (q \times r)' \rangle =$

$$\frac{1}{6} \sum_{p \in \mathcal{V}_{int}} \left(\sum_{q \text{ adjacent to } p, q \neq p} \langle v_p \times v_q, r_2 - r_1 \rangle \right),$$

where (p, q, r_2) is the properly oriented triangle in $\text{star}(\overline{pq})$, and (p, q, r_1) is the non-properly oriented triangle in $\text{star}(\overline{pq})$. Thus we have

$$\sum_{p \in \mathcal{V}} \langle p', (\nabla_p V)' \rangle = \sum_{p \in \mathcal{V}_{int}} \left(\sum_{q \text{ adjacent to } p, q \neq p} v_p^t (Q_{pq}^V) v_q \right),$$

where Q_{pq}^V is a 3×3 matrix defined as in the proposition. Thus $Q_{pp}^V = 0$, and the fact that Q_{pq}^V is skew-symmetric in p and q implies Q^V is symmetric. \square

REFERENCES

- [1] J. L. Barbosa and M. do Carmo. Stability of minimal surfaces and eigenvalues of the laplacian. *Math. Z.*, 173:13–28, 1980.
- [2] A. Bobenko and U. Pinkall. Discrete isothermic surfaces. *J. reine angew. Math.*, 475:187–208, 1996.
- [3] K. A. Brakke. Surface evolver, version 2.14. <http://www.susqu.edu/facstaff/b/brakke/evolver> or <http://www.geom.umn.edu/software/download/evolver.html>, August 1999.
- [4] S. C. Brenner and L. R. Scott. The mathematical theory of finite element methods. Springer-Verlag, 1994.
- [5] D. Bressoud and J. Propp. How the alternating sign matrix conjecture was solved. *Notices of the AMS*, 46(6):637–646, 1999.
- [6] J. Dodziuk and V. K. Patodi. Riemannian structures and triangulations of manifolds. *J. Indian Math Soc* 40:1-52, 1976.
- [7] D. Fischer-Colbrie. On complete minimal surfaces with finite Morse index in three manifolds. *Invent. Math.* 82:121-132, 1985.
- [8] G. Fix and G. Strang. An analysis of the finite element method. Prentice-Hall, 1973.
- [9] M. Gromov. Metric structures for Riemannian and non-Riemannian spaces. Progress in Mathematics, vol. 152, Springer-Verlag, 1999.
- [10] L.L. de Lima and W. Rossman. On the index of constant mean curvature 1 surfaces in hyperbolic space *Indiana Math. J.* 47(2):685-723, 1998.

- [11] S. Montiel and A. Ros. Schrödinger operators associated to a holomorphic map. *Global Differential Geometry and Global Analysis, Lect. Notes in Math. # 1481*, Berlin 1991, 147-174.
- [12] S. Nayatani. Lower bounds for the morse index of complete minimal surfaces in Euclidean 3-space. *Osaka J. Math.*, 27:453-464, 1990.
- [13] S. Nayatani. Morse index of complete minimal surfaces. *The Problem of Plateau*, ed. by Th. M. Rassias, World Scientific (1992), 181-189.
- [14] S. Nayatani. Morse index and Gauss maps of complete minimal surfaces in Euclidean 3-space. *Comment. Math. Helv.* 68:511-537, 1993.
- [15] B. Oberknapp and K. Polthier. An algorithm for discrete constant mean curvature surfaces. In H.-C. Hege and K. Polthier, editors, *Visualization and Mathematics*, pages 141–161. Springer Verlag, Heidelberg, 1997.
- [16] R. Osserman. *A Survey of Minimal Surfaces*. Dover, 1986.
- [17] U. Pinkall and K. Polthier. Computing discrete minimal surfaces and their conjugates. *Experim. Math.*, 2(1):15–36, 1993.
- [18] K. Polthier. Conjugate harmonic maps and minimal surfaces. *preprint*, 2000.

Konrad Polthier
Technische Universität Berlin
Sonderforschungsbereich 288 (Fachbereich Mathematik)
Straße des 17. Juni 136
Sekt MA 8-5, 10623 Berlin, Germany
konrad@sfb288.math.tu-berlin.de
<http://www-sfb288.math.tu-berlin.de/~konrad/konrad.html>

Wayne Rossman
Department of Mathematics
Faculty of Science
Kobe University
Rokko, Kobe 657-8501, Japan
wayne@math.kobe-u.ac.jp
<http://math.kobe-u.ac.jp/HOME/wayne/wayne.html>